JOURNAL OF APPLIED PHYSICS **113**, 187212 (2013)

Growth mechanism of photoreduced silver nanostructures on periodically proton exchanged lithium niobate: Time and concentration dependence

N. Craig Carville,[1,2] Michele Manzo,[3] Denise Denning,[1,2] Katia Gallo,[3] and Brian J. Rodriguez[1,2,a)]

[1]*School of Physics, University College Dublin, Belfield, Dublin 4, Ireland*
[2]*Conway Institute of Biomolecular and Biomedical Research, University College Dublin, Belfield, Dublin 4, Ireland*
[3]*Department of Applied Physics, KTH-Royal Institute of Technology, Roslagstullbacken 21, 106 91 Stockholm, Sweden*

(Received 2 October 2012; accepted 4 January 2013; published online 8 May 2013)

Photodeposition of metallic nanostructures onto ferroelectric surfaces, which have been chemically patterned using a proton exchange process, has recently been demonstrated. By varying the molar concentration of the $AgNO_3$ solution and the illumination time, one can determine the initial nucleation sites, control the rate of nucleation and the height of silver nanostructures formed, and study the mechanisms by which these processes occurs. The nanoparticles are found to deposit preferentially in the boundary between ferroelectric and proton exchanged regions, in an area proton exchanged via lateral diffusion under the masking layer used for chemical patterning, consistent with our previous results. Using a short illumination time (3 min), we are able to determine that the initial nucleation of the silver nanostructure, having a width of $0.17 \pm 0.02\,\mu$m and a height of 1.61 ± 0.98 nm, occurs near the edge of the reactive ion etched area within this lateral diffusion region. Over longer illumination times (15 min), we find that the silver deposition has spread to a width of $1.29 \pm 0.06\,\mu$m, extending across the entire lateral diffusion region. We report that at a high molar concentration of $AgNO_3$ (10^{-2} M), the amount of silver deposition for 5 min UV illumination is greater (2.88 ± 0.58 nm) compared to that at low (10^{-4} M) concentrations (0.78 ± 0.35 nm), however, this is not the case for longer time periods. With increasing illumination time (15 min), experiments at 10^{-4} M had greater overall deposition, 6.90 ± 1.52 nm, compared to 4.50 ± 0.76 nm at 10^{-2} M. For longer exposure times (30 min) at 10^{-2} M, the nanostructure height is 4.72 ± 0.59 nm, suggesting a saturation in the nanostructure height. The results are discussed in terms of the electric double layer that forms at the crystal surface. There is an order of magnitude difference between the Debye lengths for 10^{-2} and 10^{-4} M solutions, i.e., 3.04 vs. 30.40 nm, which suggests the Debye length plays a role in the availability of Ag^+ ions at the surface. © *2013 AIP Publishing LLC*. [http://dx.doi.org/10.1063/1.4801963]

I. INTRODUCTION

The photoreduction of metallic nanoparticles onto ferroelectric surfaces has been widely studied because of the potential applications of such structures in the electronics and biosensor industry.[1–6] The process by which photodeposition occurs, however, is still not fully understood for all surfaces, such as the initial nucleation site, the amount of deposition, and the factors that influence these, i.e., reactants concentration, time of illumination, electrostatic fields, etc. Ferroelectric materials, such as lead zirconate titanate ($Pb[Zr_xTi_{1-x}]O_3$ (PZT)),[7–9] barium titanate ($BaTiO_3$ (BTO)),[10–12] and lithium niobate ($LiNbO_3$ (LN)),[6] have been shown to be suitable ferroelectric templates for the deposition of silver nanoparticles. This is due to the photovoltaic properties these materials possess, in that when the crystals are exposed to a superbandgap energy source, photogenerated electron-hole pairs are created.[13] These photogenerated electrons can contribute to reduction reactions occurring at the surface, e.g., $Ag^+ + e^- = Ag^0$. The process by which this occurs has been shown to depend on a range of factors, such as polarization-mediated effects (Stern layer, screening, band bending, etc.)[13,14] and on the experimental conditions (concentration, illumination intensity, time, wavelength, etc.).[15] Recent work by Sun *et al*. has demonstrated that the Ag deposition on periodically poled LN (PPLN) is dependent on the concentration of $AgNO_3$ and the power intensity of UV light source.[15] They show that controlling the ratio of Ag^+ ions and photon flux (flux ratio) by increasing the reactants concentration (10^{-3}M) and lowering the UV intensity ($1400\,\mu W/cm^2$), results in enhanced nanowire-like structures on the 180° domain boundary. In contrast, they report that a lower concentration (10^{-7}M) decreases the flux ratio and results in a more uniform distribution of deposition along the positive and negative domains, and suppressed deposition along the domain wall boundaries.[15]

Our approach involves the use of a surface chemical grating of proton exchange (PE), which ultimately affects the surface ferroelectric and piezoelectric properties.[16] Chemical patterning creates regions of different ferro- and piezoelectric properties as opposed to domain patterning techniques,

a)Author to whom correspondence should be addressed. Electronic mail: brian.rodriguez@ucd.ie

which create oppositely poled domains. The periodic alteration of the surface properties changes the electrostatic fields at the boundary between these regions, and photodeposited structures are confined to this boundary region.[17,18] The inclusion of the protons in the crystalline lattice ($H_xLi_{1-x}NbO_3$)[19–21] through the PE process results in abrupt variations of the intrinsic polarization between the PE/non-PE regions, which lead to the generation of strong electrostatic fields beneath the crystal surface.[17] Typically, in PPLN, the highest electric field arising from the sudden variation of the polarization is confined across a thin region across the 180° domain boundary,[6] whereas in our samples, the fabrication process yields a transition region between the LN crystal (ferro- and piezoelectric) and PE (reduced ferro- and piezoelectric properties) called lateral diffusion (LD).[18] In this region, the electric field generated by the polarization modulation due to PE (Ref. 17) is enhanced, and thus, can be exploited via the photovoltaic effect. Our previous work[18] has shown that when the sample is immersed in aqueous silver nitrate ($AgNO_3$, 10^{-2} M) and illuminated with super-bandgap energy light ($E > E_{gLN} = 3.9$ eV, corresponding to a wavelength $\lambda < 318$ nm), electrons are made available for reduction reactions. This suggests that in the LD region, where static electric fields are embedded, the photogenerated electron-hole pairs are separated. The electrons generated in this region can then partake in the silver reduction reaction, thus, leading to selective silver deposition onto the LD region at the crystal surface. The growth mechanism and nucleation of silver particles using this technique, however, have not been previously addressed. Here, we analyze these key points by exploring the role of the concentration of $AgNO_3$ and UV illumination time on the amount of deposition. This enables us to control the height of the nanostructures, and gives us further insights into the mechanisms involved in photochemical reactions on chemically patterned ferroelectric templates, which can offer additional degrees of freedom (besides periodic poling techniques) to pattern ferroelectric templates for new applications in, e.g., biological sensing, which could exploit the combined electrical, optical, and plasmonic functionalities of hybrid ferroelectric-metallic structures.

II. EXPERIMENTAL

We used 500 μm-thick z-cut optical grade congruent LN as ferroelectric substrates. The selective chemical patterning of the +z surface of the crystal was performed via PE through the openings of a periodic metallic (titanium) mask deposited and patterned on the crystal surface prior to the PE step. The Ti pattern, defined by standard photolithography and reactive ion etching (RIE), had a period $\Lambda = 6.09\,\mu$m and contained periodic openings of a width $w_{RIE} = 2.4\,\mu$m. PE was performed through those Ti openings by dipping the samples in molten pure benzoic acid for 24 h at 200 °C. The resulting periodic pattern at the crystal surface consisted of pure (LN) and proton-exchanged (PE) stripes, with widths $w_{LN} \sim 0.95\,\mu$m and $w_{PE} \sim 5.15\,\mu$m, respectively. Within each PE stripe, we identify a central region (w_{RIE}), corresponding to the opening of the mask through which PE was performed, and two lateral ones (w_{LD}), corresponding to areas of the crystal which, despite being covered by the Ti mask, were still subject to PE (since proton diffusion proceeds not only in depth but also sideways from the mask openings) as highlighted in Ref. 18. These two types of PE regions can give rise to qualitatively different behavior during Ag-photodeposition. We shall use the labels "RIE" and "LD" (as lateral diffusion) to discriminate between them in what follows. After PE, the Ti was removed through wet-etch in a dilute HF:H_2O solution for a few seconds, the resulting sample is subsequently referred to as periodic proton exchanged LN (PPELN). The electrostatic field formed at the PE:LN interface is depicted in Figure 1(a). At 10 nm above the surface, the in-plane component of the electric field (E_x) is maximum at the boundaries between the LD and LN regions.

Before photodeposition, the samples were sonicated for 20 min in acetone, 20 min in isopropanol (IPA), and 20 min in Milli-Q water (18.2MΩ cm^{-1}). To study the topographical and piezoelectric properties of the sample before deposition, amplitude modulation mode atomic force microscopy (AFM) and piezoresponse force microscopy (PFM) (Asylum

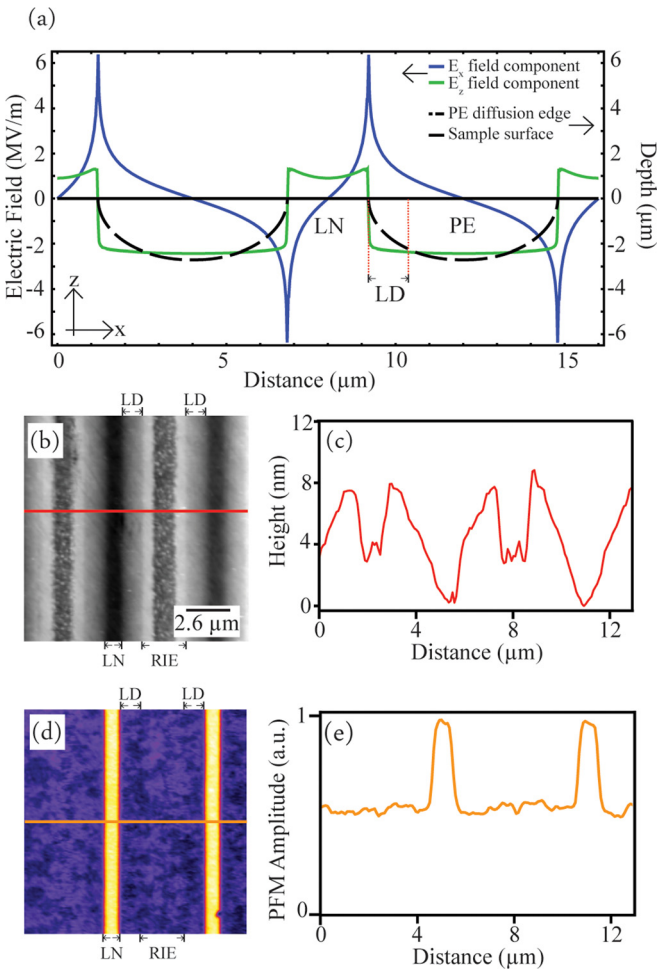

FIG. 1. (a) Electrostatic field simulation of an ideal PPELN surface showing the in-plane (E_x) and out-of-plane (E_z) electric field components 10 nm above the surface. (b) AFM topography image and (c) corresponding line profile of the +z PPELN surface prior to photodeposition. (d) PFM amplitude image and (e) corresponding line profile. The proton exchanged region comprises LD and RIE regions.

Research, MFP-3D), respectively, were carried out. The topographical measurements were carried out using a nonconducting tip (Nanosensors, PPP-NCH) with a resonant frequency of 318 kHz and a spring constant of 29 N/m. For the PFM measurements, a 6 V AC voltage (modulated at 600 kHz) was applied to a conductive tip (Nanosensors, PPP-NCHAu) with a resonant frequency of 196 kHz and a spring constant of 18 N/m) during contact mode imaging. When an external electric field is applied to the crystal, the surface deforms due to the converse piezoelectric effect. These surface deformations result in deflections of the AFM cantilever at the modulation frequency, which are recorded and demodulated into amplitude and phase signals using a lock-in amplifier (Zurich Instruments, HF2LI). From PFM amplitude signal, it is possible to determine the amplitude of the biased tip induced deformations occurring at the surface. PFM is a useful technique for distinguishing between regions having different piezoelectric properties such as LN and PE:LN.

As previously mentioned, photodeposition of metallic nanowires on LN surfaces occurs as a result of the following reaction: $Ag^+ + e^- = Ag^0$, whereby the Ag^+ ions from the $AgNO_3$ solution are reduced by photogenerated electrons from the substrate. Critical parameters for the process are accordingly the (electron-generating) photon flux (J_{ph}) and the metal ion flux (J_i), as well as their ratio. For a given intensity (I_0) and wavelength (λ) of the UV illumination source, the photon flux, J_{ph} (photons/cm^2 s), which drives the electron generation, can be calculated from[15]

$$J_{ph} = \frac{I_0 \times \lambda}{h \times c}, \tag{1}$$

where h is Planck's constant, and c is the speed of light.

To determine the metal ion flux, an approach commonly used[15] is the one presented by Anderson and Feldberg.[22] The chemical flux density, J_i (ions/cm^2 s), of a solution is calculated using the following equation:

$$J_i = v_0 C_0, \tag{2}$$

where v_0 is the average velocity toward a surface of a single particle in solution and C_0 is the concentration of the particles in solution near the LN surface. The average velocity v_0 is the surface collision velocity within a mean free path distance from the surface, however, it is not dependent on the solvent properties, i.e., viscosity, and can be calculated assuming an ideal gas.

The photodeposition experiments were performed using a fixed intensity and wavelength for the UV source (Spectroline lamp, see below), providing a constant photon flux. We varied the metal ion flux by varying the $AgNO_3$ concentration in the bulk solution (C_0), according to Eq. (2). We prepared solutions with $C_0 = 10^{-2}$, 10^{-3}, and 10^{-4} M, obtained by diluting the stock solution 10^{-2} M $AgNO_3$ (Sigma Aldrich) in Milli-Q water. The values of C_0 and J_i are listed in Table I.

The sample was placed on a glass slide inside a petri dish, and 160 μl of each solution was pipetted onto the surface. The sample was then illuminated at a wavelength $\lambda = 254$ nm with a penlamp (Spectroline) located 2 cm above the surface yielding $I_0 = 2$ W/cm^2 illumination intensity. The corresponding photon flux calculated from Eq. (1) is $J_{ph} = 2.57 \times 10^{15}$ (photons/cm^2 s). Photons at a wavelength of 254 nm possess energy that is higher than both the LN bandgap (>3.9 eV)[23] and the PE:LN bandgap (>3.65 eV) as determined from spectroscopic UV edge measurements,[18] being then suitable for the generation of electron hole pairs on the surface.

TABLE I. Parameters for $AgNO_3$ concentration, flux calculations, and resulting deposition heights obtained for an illumination time of 15 min. The UV intensity was kept constant at $I_0 = 2$ mW/cm^2, corresponding to a photon flux $J_{ph} = 2.57 \times 10^{15}$ photons/cm^2 s.

Concentration (M)	1×10^{-2}	1×10^{-3}	1×10^{-4}
Metal ion flux, J_i (ions/cm^2 s)	1×10^{22}	1×10^{21}	1×10^{20}
Flux ratio (J_i/J_{ph})	3.89×10^6	3.89×10^5	3.89×10^4
Average height of deposition (nm)	4.50 ± 0.76	5.28 ± 0.45	6.90 ± 0.92
Debye length (nm)	3.04	9.61	30.40

Another important parameter for the photodeposition is the UV exposure time. To study its impact, we fixed the concentration (to 10^{-2} M) and chose five illumination times: $\Delta\tau = 3$, 5, 10, 15, and 25 min.

After deposition, the samples were imaged again using the same tips and in amplitude modulation mode AFM. After imaging, the samples can be reused by cleaning with the same protocol mentioned before, but using IPA soaked lens paper between the acetone and IPA stage and gently rubbing the sample. Before any other deposition experiment, the sample is imaged using AFM to ensure all silver has been removed from the surface. The analysis of the images was carried out using WSXM.[24] Each image was aligned with the 1-dimensional stripe pattern parallel to the y-axis, and subsequently y-averaged to create an averaged cross section. Line profiles are cross sections perpendicular to the periodic pattern and parallel to the x-axis.

III. RESULTS

The photoreduction of silver on PPELN samples was carried out via $AgNO_3$ immersion and UV illumination. To study the mechanism by which this occurs, and to show controllability of the deposition height, we vary the concentration of solution and the time of illumination. The PPELN sample was imaged before deposition (Figure 1(b)). The topographical features are due to the fabrication process of the Ti mask and successive PE.[18] On inspection of the AFM image (Figure 1(b)) and corresponding line profile (Figure 1(c)), the periodically pure LN and PE regions can be properly identified. The LN regions appear as the darkest ones, i.e., the lowest regions in the line profile (Figure 1(c)), whereas the PE region can be identified as the wider "swollen" region containing characteristic groove-like features. The swelling is a consequence of the stress associated with the inclusion of protons in the crystal lattice.[25] The groove-like structures located on top of the swollen regions mark the original Ti openings and are produced by the slight

RIE over etch of LN during mask fabrication. The PE region is wider than the original Ti openings due to the lateral diffusion of protons under the Ti mask, as mentioned before.

The piezoelectric properties of the surface were characterized using PFM (Figures 1(d) and 1(e)). From the normalized PFM amplitude image (Figure 1(d)), and the corresponding line profile (Figure 1(e)), the areas with highest piezoresponse are identified as the non-PE regions, i.e., pure LN, while the regions with reduced piezoresponse correspond to the PE sections, as the inclusion of protons reduces the spontaneous polarization and hence also the piezoelectric properties of the crystal.[26]

After exposure to $AgNO_3$ solutions of varying concentration and fixing the UV illumination time to 15 min, the sample is imaged using AFM to track the surface variations, which are illustrated in Figures 2(a)–2(c). The results clearly support the notion that the silver photoreduction occurs in the area between the PE-RIE and LN regions, namely the PE-LD portion.[18] This is even more evident in Figure 2(d), which shows the *y*-averaged line profiles for each concentration. From the line profiles, it is possible to calculate the average heights of the deposited region. For the different concentrations, 10^{-2}, 10^{-3}, and 10^{-4} M, the heights were 9.96 ± 0.89, 11.35 ± 0.71, and 13.22 ± 0.92 nm ($\pm$standard deviation, $n = 40$), respectively. These values do not represent the actual thickness of the deposition, but rather both the change in thickness due to PE-induced swelling and the thickness of the deposition. Table I represents the actual thickness of deposition, and the values were calculated from the data illustrated in Figure 2(d) but subtracted from the *y*-averaged profile of the before deposition image. The roughness analysis shows a similar trend where the higher concentration (10^{-2}) is less rough, 1.94 nm RMS, compared to the lowest concentration (10^{-4}), 4.03 nm RMS, in the deposited region. The preferential deposition on the LD region is evident in all cases, and the roughness analysis of the LN and RIE regions shows that the values are within 0.5 nm RMS of each other, which is also the case for the AFM topography image of the sample before deposition.

The next step is to investigate the influence of the illumination time by keeping the reactants concentrations constant. The result of such experiment is imaged in Figures 3(a)–3(d) which illustrates the AFM topography at the same concentration (10^{-2} M $AgNO_3$) at different exposure times. It is evident from Figure 3(a) that the initial nucleation of silver occurs at the interface between the LD region and the RIE region with a width of $0.17 \pm 0.02\,\mu$m and as the time increases the silver deposits on the whole LD region reaching a width of $1.29 \pm 0.06\,\mu$m. Figure 3(e) illustrates the resulting Ag nanoparticle morphology for an illumination time of 5 min. In Figure 3(f), the *y*-averaged line profiles for the different time points are overlaid, which shows the differences more quantitatively. The amount of deposition increases rapidly up until around 25 min and this is where the thickness of the deposition appears to saturate, in that the height of the line profile remains at around 12 nm. This is evident from the line profiles in Figure 3(f), and also in the *y*-averaged line profiles (subtracted from the before deposition profile) in Figure 4(a). To compare the amount of deposition across all concentrations, three time points were taken,

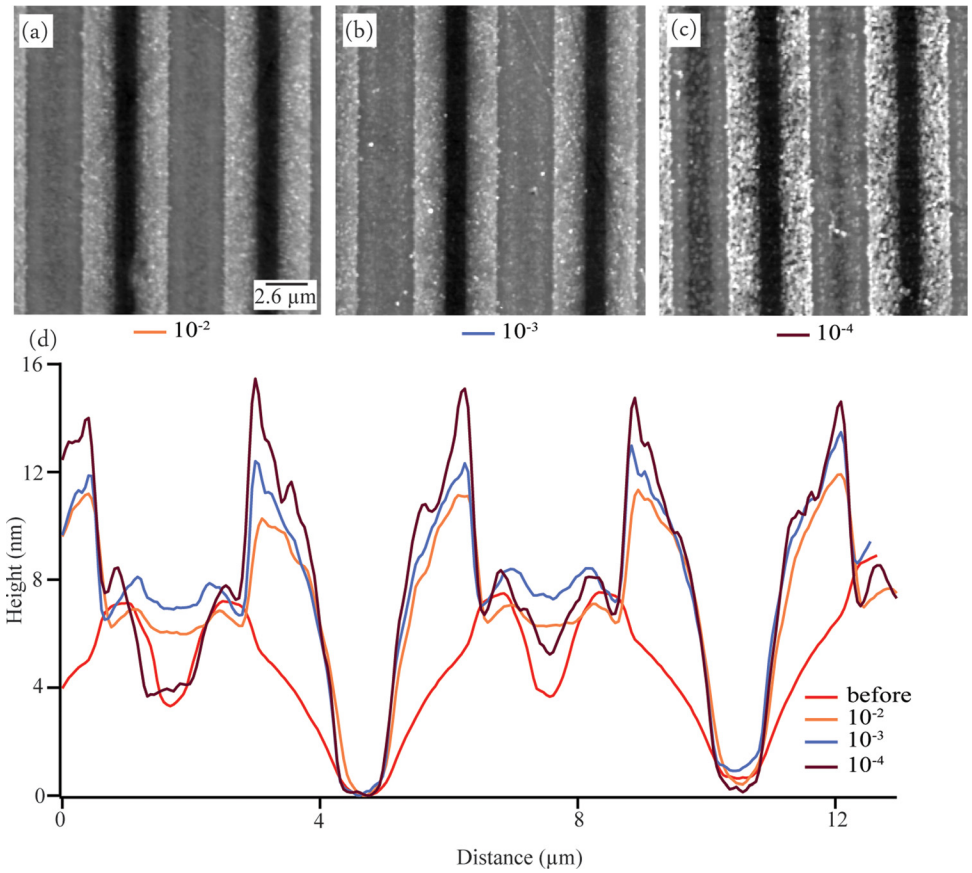

FIG. 2. (a)–(c) AFM topography images from the concentration study on +z PPELN surface with 10^{-2}, 10^{-2}, and 10^{-3} M $AgNO_3$, respectively, with an illumination time of 15 min. (d) An overlay of *y*-averaged line profiles from the AFM topography images.

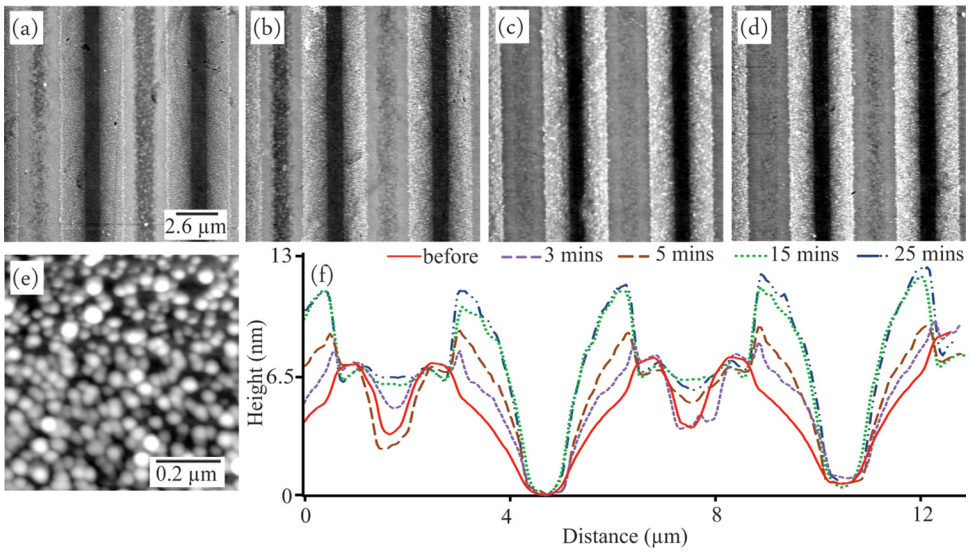

FIG. 3. (a)–(d) AFM topography images from the time study on +z PPELN surface with 10^{-2} M $AgNO_3$ for 3, 5, 15, and 25 min, respectively. (e) AFM topography image (0.7 μm scan size) on the LD region after illumination for 5 min. (f) An overlay of *y*-averaged line profiles from the above AFM topography images.

of 5, 10, and 15 min, respectively, at each concentration. The results are illustrated in Figures 4(a) and 4(b), which refers to measurements taken in the LD region. Each data point represents the amount of deposition after illumination (estimated by subtracting the LN surface topography as determined from the before-illumination image, see Figure 1(b)). After 5 min, more silver deposition can be seen for the higher concentration compared to the lower concentrations,

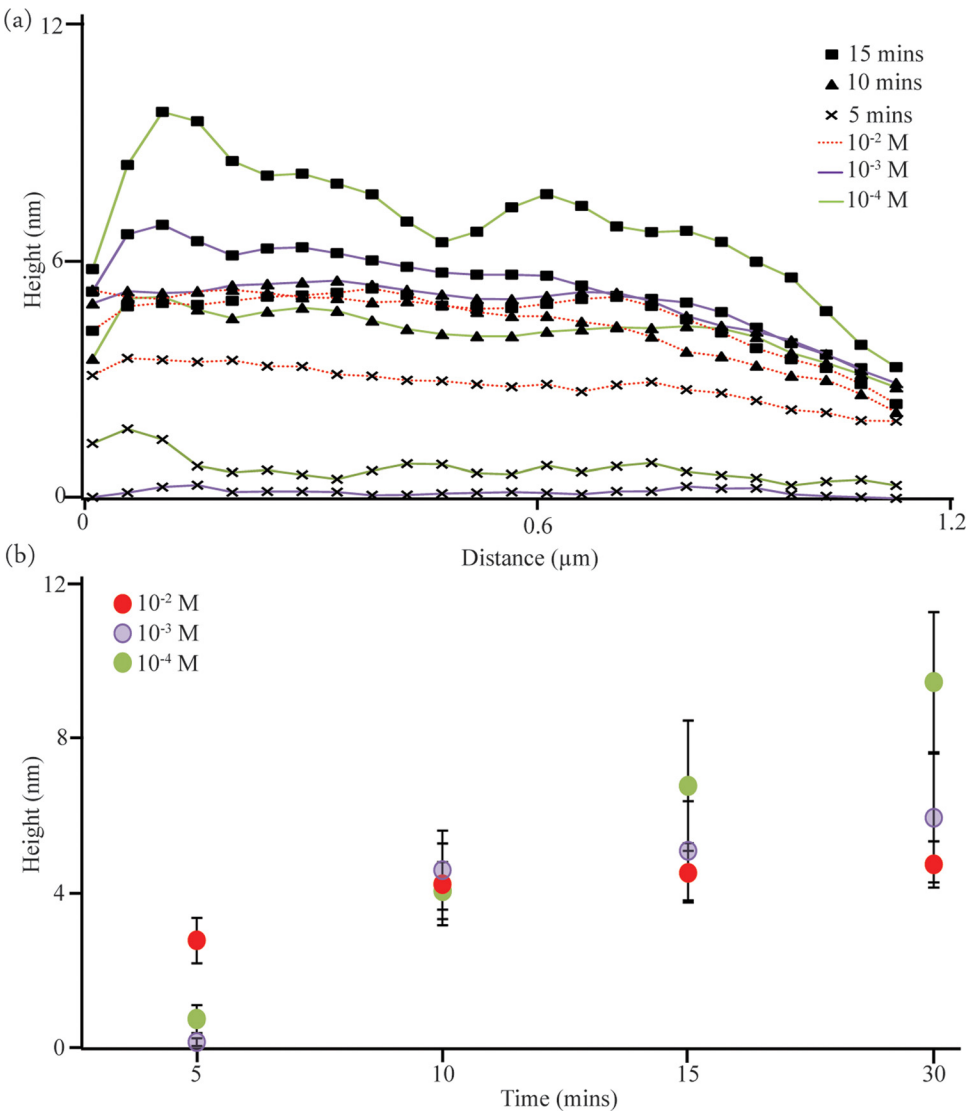

FIG. 4. (a) Comparison of *y*-averaged line profiles (subtracted from the before deposition profile) for each concentration and overlaid for the lateral diffusion region for one period. (b) The average height of the nanostructures formed in the lateral diffusion region from (a) with standard deviation shown, as a function of time for concentrations 10^{-2} M (red circle), 10^{-3} M (purple circle), and 10^{-4} M (green circle).

however, this is not the case for all time points. After 10 min illumination, all concentrations are within 0.6 nm of each other. For 15 min, as highlighted previously, the amount of deposition is increased for the lower concentrations as compared with the high concentration. This is the opposite response to what we see at 5 min illumination time. Figure 4(b) illustrates the average height for each time point and concentration, which shows the same trend as Figure 4(a).

IV. DISCUSSION

It is known from previous studies that the photochemistry on ferroelectric surfaces is dictated by the surface electric field distribution, which is controlled by polarization and influenced by defects.[6,13] Previous experiments employing PPLN substrates as a template for photoreduction showed a pronounced nanowire-like metallic silver deposition occurring at the 180° domain boundaries, as a result of maximized surface electric field in these regions.[6,15] In our previous work,[18] we have shown that the deposition of silver nanoparticles can be controlled by patterning electrostatic field distributions at the LN crystal surface via a selective chemical treatment, namely proton-exchange. Both the arrangement and the influx of protons in the PPELN substrate change the ferro- and piezoelectric properties of the surface, which in turn affects the polarization and the electric field distributions. The effects of such engineered built-in electrostatic field distributions in PPELN[17] are shown to be concentrated in the LD region (at the transition between LN and the highest proton concentration region, corresponding to direct PE from the melt). Illumination with super-bandgap light generates electron-hole pairs which are separated by the electric fields embedded in the crystal. In particular, the silver deposition occurs preferentially on the LD region (Figure 2), suggesting electrons present (via photogeneration or drift) on the LD region partake in the reduction of silver.

In order to fully understand and control the deposition rates and features, it is important to characterize how the nucleation of silver is influenced by the illumination time and the concentration of $AgNO_3$. The impact of varying illumination times is illustrated in Figures 3(a)–3(d). In the initial time period of 3 min, the deposition occurs via nanowire-like formations (width $0.17 \pm 0.02\ \mu$m) on the PE-LD region, at the edge of the RIE boundary. This preferential deposition can be attributed to the asymmetric electric field distribution across the LD region (correlated to PE gradients in depth and in the lateral direction),[21] and also to differences in bandgap between LN and PE regions and variation in topography.[23] Over time, however, the nucleation of metal spreads out over the whole LD region ($1.29\ \mu$m), which likely results from more electrons being available for the reduction (hence enabling deposition also in areas where the electrostatic fields are reduced), yet still keeping the high selectivity between LN (essentially no deposition) and PE areas.

Next, a concentration study was performed (Figure 2). The results suggest that having a lower concentration of $AgNO_3$ gives a higher amount of silver deposition over 15 min as compared with a higher concentration. Further studies are needed to assess the impact of scattering/absorption by the Ag structures already in place on the actual photon flux reaching the crystal surface as deposition progresses. Additional unknowns derive from potential modification of the ion flux at the surface during the Ag growth. Nevertheless, to analyze the experimental results, one can start with a simplified model (as used by Sun *et al*. for the case of Ag photodeposition on PPLN).[15]

In order to explain the differences in the reported results, one has to take into consideration the parameters used, which influence the metal ion flux (amount of Ag ions impinging on the surface) and the photon flux (affecting the amount of electrons available). The metal ion flux and photon flux are calculated from Eqs. (1) and (2) (shown in Table I), from which the ratio of the fluxes can be obtained. For the case where there are more metal ions than electrons available, the silver deposition will be limited by the number of electrons, i.e., the deposition operates under an electron-limited regime. In comparison, when there are more electrons available than metal ions, deposition will be limited by the number of metal ions, i.e., an ion-limited regime. The real ion flux will be mediated by the electrical double layer.[15] The amount of electrons inferred from the photon flux will depend both on the efficiency of electron-hole pair generation, and on the presence of photodeposited metal. It will also be affected by Rayleigh scattering.[27] As the concentration of $AgNO_3$ increases, the scattering of photons is also increased, thus, reducing the incident photon flux. For all of the concentrations studied, the metal ion flux is greater than the photon flux. Thus, there may not always be an electron available to partake in the reduction reaction. In order to probe the ion-limited regime, a lower concentration is required (limited by the purity of the Milli-Q water), or, e.g., the electrical double layer will need to disrupt the ion flux by a factor of 10^4.

Figure 4 illustrates that the silver deposition thickness is greater for the highest concentration at the shortest time, and in contrast, for the lowest concentration at the longest time. As the metal ion flux is greater than the corresponding number of available electrons, even assuming an electron hole pair conversion efficiency of 1, another mechanism must dictate the thickness of the photodeposited silver nanostructures. The bound polarization surface charge of ferroelectric materials will be screened partially by external charge, in our case, coming from the aqueous $AgNO_3$ solution. As a result, an electrical double layer will form. Considering the experiment is performed on the $+z$ surface of the crystal, it is expected that NO_3 anions and polarized water molecules will be strongly attracted to the surface.[2,9] We calculate the Debye length for the highest and lowest concentrations to be 3.04 nm and 30.40 nm, respectively. These values correlate with the measured deposition heights. For the highest concentration, the thickest deposition is 4.72 ± 0.59 nm for an exposure time of 30 min. This suggests the crowding of NO_3^- ions at the surface decreases the availability of the Ag^+ ions for reduction reactions. Thus, for the highest concentration, the height of the nanostructure appears to be limited by the Debye length. For the lowest concentration, the height of the structure surpasses its higher

concentration counterpart after around 10 min of UV exposure. The deposition height increases roughly linearly with time and does not saturate for exposure times up to 30 min. To fully understand the interplay between Debye length and Raleigh scattering on $AgNO_3$ concentration dependent UV absorption and photodeposition, further investigations, particularly for longer times, are required.

V. CONCLUSION

We have demonstrated the initial growth mechanisms by which silver nanostructures nucleate and assemble on chemically patterned LN crystals by controlling the amount of time for illumination. We have also demonstrated the controllability of the nanostructure height by varying the concentration of $AgNO_3$. The results obtained show that for high concentrations (10^{-2} M) the amount of deposition was greatest for the initial exposure time (5 min), however, for longer exposure times, the lower concentration (10^{-4} M) gave the greatest amount of deposition. The variations in deposition heights correlate with the Debye length, which is an order of magnitude higher for 10^{-4} M compared to 10^{-2} M. These results show that it is possible to control the deposition height by varying the illumination time and concentration. The embedded electric fields in the PPE crystal are the greatest factor determining where the silver deposits for the experimental parameters explored in this work, as demonstrated via the selectivity of the deposition in the LD regions. The initial nucleation of silver, however, occurs at the interface between the RIE region and LD region, which could result from, e.g., the asymmetric electric field distribution across the LD region arising from the topographical gradient of PE depth and the lateral diffusion or an electric double layer disturbance caused by a surface feature, as demonstrated previously on PZT.[9] Further studies are needed to fully understand this phenomenon. The results presented provide more insight to the deposition on chemically patterned LN, as we can control the nanostructures height. Being able to control the height and amount of silver deposition can may make way for further work into applications of these surfaces i.e., having more silver could increase the surface area for metal adsorption of molecules, which would increase sensitivity of detection in sensors.

ACKNOWLEDGMENTS

This publication has emanated from research conducted with the financial support of the DGPP and NANOREMEDIES, which are funded under the Programme for Research in Third Level Institutions (PRTLI) Cycle 5 and co-funded by the European Regional Development Fund. This work was also supported by Science Foundation Ireland (SFI10/RFP/MTR2855), the Swedish Scientific Research Council (VR 622-2010-526 and 621-2011-4040), and the ADOPT Linné Center for Advanced Optics and Photonics. The authors are grateful to COST actions MP0702 and MP0904. The AFM used for this work was funded by Science Foundation Ireland (SFI07/IN1/B031).

[1]S. Dunn, S. Sharp, and S. Burgess, Nanotechnology **20**, 115604 (2009).
[2]S. Dunn, P. M. Jones, and D. E. Gallardo, J. Am. Chem. Soc. **129**, 8724 (2007).
[3]X. Y. Liu, K. Kitamura, K. Terabe, H. Hatano, and N. Ohashi, Appl. Phys. Lett. **91**, 044101 (2007).
[4]X. Y. Liu, F. Ohuchi, and K. Kitamura, Funct. Mater. Lett. **1**, 177 (2008).
[5]S. Dunn and D. Tiwari, Appl. Phys. Lett. **93**, 092905 (2008).
[6]J. N. Hanson, B. J. Rodriguez, R. J. Nemanich, and A. Gruverman, Nanotechnology **17**, 4946 (2006).
[7]P. Jones and S. Dunn, Nanotechnology **18**, 185702 (2007).
[8]P. Jones, D. E. Gallardo, and S. Dunn, Chem. Mater. **20**, 5901 (2008).
[9]P. M. Jones and S. Dunn, J. Phys. D: Appl. Phys. **42**, 065408 (2009).
[10]S. V. Kalinin, D. A. Bonnell, T. Alvarez, X. Lei, J. H. Ferris, Q. Zang and S. Dunn, Nano Lett. **2**, 589 (2002).
[11]J. L. Giocondi and G. S. Rohrer, Chem. Mater. **13**, 241 (2001).
[12]S. V. Kalinin, D. A. Bonnell, T. Alvarez, X. Lei, Z. Hu, R. Shao and J. H. Ferris, Adv. Mater. **16**, 795 (2004).
[13]D. Tiwari and S. Dunn, J. Mater. Sci. **44**, 5063 (2009).
[14]Y. Sun and R. J. Nemanich, J. Appl. Phys. **109**, 104302 (2011).
[15]Y. Sun, B. S. Eller, and R. J. Nemanich, J. Appl. Phys. **110**, 084303 (2011).
[16]J. L. Jackel, C. E. Rice, and J. L. Veselka, Appl. Phys. Lett. **41**, 607 (1982).
[17]M. Manzo, F. Laurell, V. Pasiskevicius, and K. Gallo, Appl. Phys. Lett. **98**, 122910 (2011).
[18]N. C. Carville, M. Manzo, S. Damm, M. Castiella, L. Collins, D. Denning, S. A. L. Weber, K. Gallo, J. H. Rice, and B. J. Rodriguez, ACS Nano **6**, 7373 (2012).
[19]R. G. Wilson, S. W. Novak, J. M. Zavada, A. Loni, and R. M. De La Rue, J. Appl. Phys. **66**, 6055 (1989).
[20]Yu. N. Korkishko and V. A. Fedorov, *Ion Exchange in single Crystals for Integrated Optics and Optoelectronics* (Cambridge International Science Publication, Cambridge, 1999), pp. 127–143.
[21]R. V. Roussev, V. Bhagavatula, J. Himmelreich, K. Becken, and J. Tingley, Proc. SPIE **7917**, 79171Z (2011).
[22]O. S. Andersen and J. Feldberg, J. Phys. Chem. **100**, 4622 (1996).
[23]A. M. Prokhorov and Y. S. Kuzminov, *Crystalline Lithium Niobate* (Adam Hilger, New York, 1990).
[24]I. Horcas, R. Fernandez, J. M. Gomez-Rodriguez, J. Colchero, J. Gomez-Herrero, and A. M. Baro, Rev. Sci. Instrum. **78**, 013705 (2007).
[25]F. Zhou, A. M. Matteo, R. M. De La Rue, and C. N. Ironside, Electron. Lett. **28**, 87 (1992).
[26]C. E. Rice and M. Hill, Mater. Res. Bull. **19**, 591 (1984).
[27]A. Quirantes, F. Arroyo, and J. Quirantes-Ros, J. Colloid Interface Sci. **240**, 78 (2001).